ELSEVIER

Contents lists available at ScienceDirect

# Colloids and Surfaces A: Physicochemical and Engineering Aspects

journal homepage: www.elsevier.com/locate/colsurfa



# Sucrose monolaurate self-assembly via hydrogen bonding: Role of surfactant concentration and urea

N. Pagureva <sup>a,1</sup>, F. Mustan <sup>a,b,1</sup>, D. Cholakova <sup>a</sup>, N. Burdzhiev <sup>c</sup>, A. Ivanova <sup>d</sup>, S. Tcholakova <sup>a,\*</sup>

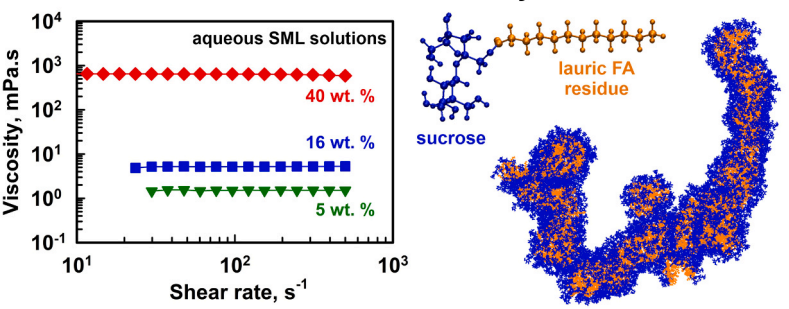
- a Department of Chemical and Pharmaceutical Engineering, Faculty of Chemistry and Pharmacy, University of Sofia, 1 James Bourchier Ave., Sofia 1164, Bulgaria
- b Centre of Competence "Sustainable Utilization of Bio-resources and Waste of Medicinal and Aromatic Plants for Innovative Bioactive Products" (BIORESOURCES BG), Sofia, Bulgaria
- c Department of Organic Chemistry and Pharmacognosy, Faculty of Chemistry and Pharmacy, University of Sofia, 1 James Bourchier Ave., Sofia 1164, Bulgaria
- d Department of Physical Chemistry, Faculty of Chemistry and Pharmacy, University of Sofia, 1 James Bourchier Ave., Sofia 1164, Bulgaria

#### HIGHLIGHTS

- ullet Sucrose monolaurate self-assembly in water  $\pm$  urea is investigated.
- Formation of spherical micelles is observed between 1 and 40 wt%.
- All solutions have Newtonian behavior, with viscosity increasing sharply above
  20 wr%
- H-bonding drives micelle aggregation into thread-like structures, while preserving micelle individuality.
- Addition of urea disrupts the H-bonds, leading to reduced structural organization.

#### GRAPHICAL ABSTRACT

# Sucrose monolaurate micelles self-assembly via H-bonds formation



# ARTICLE INFO

Keywords: Sucrose ester Micelle Phase behavior Molecular dynamics Rheology Pearl necklace

# $A\ B\ S\ T\ R\ A\ C\ T$

Sugar esters, a class of surfactants derived from renewable resources, have attracted significant attention due to their biodegradability, low toxicity, and broad applications in food, cosmetic, and pharmaceutical formulations. Despite their widespread use, the phase behavior of these compounds in aqueous systems remains incompletely understood. In this study, we investigate the self-assembly of a nonionic sucrose ester of lauric acid in 1–40 wt% concentration range using rheological measurements, dynamic light scattering, X-ray scattering, DOSY NMR, and molecular dynamics simulations. Formation of spherical micelles with a diameter of 5.4 nm is observed at low surfactant concentrations, driven by hydrophobic interactions between the alkyl tails. These solutions exhibit Newtonian flow behavior with viscosities close to that of pure water. However, the viscosity increases from 5 mPa.s at 16 wt% to 640 mPa.s at 40 wt%, while the Newtonian character persists even at 40 wt%. This behavior is explained with the formation of interconnected, thread-like micellar structures of (almost) spherical micelles that largely preserve their distinctiveness, resembling the "pearl necklace" arrangement known for polymer systems. The main driving force for this supramolecular organization was found to be the hydrogen bonding between sucrose headgroups. The addition of 6 M urea, a known hydrogen bond disruptor, significantly reduces micelle clustering and the viscosity decreases to 150 mPa.s at 40 wt% concentration, supporting the proposed

E-mail address: sc@lcpe.uni-sofia.bg (S. Tcholakova).

#### https://doi.org/10.1016/j.colsurfa.2025.138915

<sup>\*</sup> Corresponding author.

<sup>&</sup>lt;sup>1</sup> These authors contributed equally to this paper

aggregation mechanism. These findings contribute to a deeper understanding of the self-assembly behavior of sucrose esters in aqueous environment and highlight their potential for controlled aggregation in practical formulations.

#### 1. Introduction

Currently, there is a high demand to replace the synthetic petrochemically derived surfactants in different formulations by more ecofriendly, sustainable 'green' substances [1-4]. A prominent candidate for the replacement of the widely used nonionic alcohol ethoxylated surfactants are the alkyl sucrose esters. Sucrose esters, derived upon esterification of sucrose with fatty acids [4-7], are known to have numerous beneficial properties, including being biodegradable, biocompatible, non-toxic, tasteless and odorless [4,5,8-11]. Furthermore, they are shown to possess antimicrobial activity, insecticidal, anti-inflammatory, antitumor and antioxidant properties and to be able to serve as permeability enhancers for drug molecules [5,8,12,13]. Sucrose esters can be synthesized using fatty acids with varying chain lengths, whereas the mono- to polyesters ratio present within the obtained surfactant mixture determines their hydrophilic-lipophilic properties, rendering them suitable for both oil- and aqueous-based products [8,14]. All these characteristics make the sucrose esters widely studied and used in various food, cosmetic, detergent and drug delivery formulations [15-20].

Although the phase behavior of sucrose esters in water has been widely investigated [21–27], some of the fundamental mechanisms behind the experimentally observed behavior still lack an in-depth understanding. For example, it has recently been shown that the viscosity of the long-chain sucrose palmitate surfactant P1670 (containing ca. 80 % monoesters, 20 % diesters and  $C_{16}$ -to- $C_{18}$  fatty acid residues ratio  $\approx$ 3:1) passes through a maximum upon heating. This was explained with the melting of the diester particles present in the solution at low temperatures and formation of mixed wormlike micelles together with the monoesters [28]. The presence of the diester particles was later found to be responsible for the ability of sucrose esters dispersions to form completely non-flowing gel-like samples at very low surfactant and salt concentrations, e.g. 1.5 wt% surfactant and 10 mM NaCl [29]. This phenomenon arises due to the adsorption of hydroxide anions from the water onto the surface of the in-situ prepared nonionic surfactant particles, making them negatively charged, hence susceptible to the presence of electrolyte [29].

Another non-trivial behavior deserving further investigation is the significant viscosity increase (by more than 2 orders of magnitude) observed in aqueous sucrose laurate solutions upon increase of the surfactant concentration. Such behavior has been reported in Ref. [30]. However, the solutions prepared with sucrose laurate contents up to 45 wt% were reported to be isotropic and showed Newtonian viscous liquid behavior [30]. Therefore, the molecular arrangement of sucrose laurate in solution responsible for the pronounced viscosity increase, yet maintaining Newtonian behavior, remains unresolved.

The aim of this study is to investigate the concentration-dependent molecular arrangement of sucrose laurate in water and to determine the mechanisms leading to the significant viscosity increase upon increase of the surfactant concentration up to 40 wt%, while the Newtonian rheological behavior of the samples is preserved. For that purpose, we performed rheological and structural (SAXS) measurements, NMR experiments, as well as molecular dynamics simulations. The results showed a notable effect of the presence of hydrogen bonds between the sucrose headgroups. Hence, further experiments were performed in presence of the hydrogen-bond-breaking agent urea to understand its impact over the observed behavior.

#### 2. Materials and methods

#### 2.1. Materials

Dodecyl sucrose ester (trade name L1695, Ryoto<sup>TM</sup>) was obtained by Mitsubishi Chemical Group and was used as received in the experiments. HPLC analysis performed in our lab showed that this surfactant contains about 87 % monoesters and 13 % polyesters (the main fraction being the diesters). The alkyl chains in the L1695 surfactant were found to be of high purity, with more than 99 % being lauric ( $C_{12}$ ) [31]. Urea (purity > 99.5 %) was obtained from Riedel de Haen (Honeywell International Inc., USA).

All solutions were prepared using deionized water purified with an Elix 3 system (Merck-Millipore Inc., USA).

## 2.2. Experimental methods

#### 2.2.1. Solutions preparation

To prepare the L1695 surfactant solutions, the required amount of surfactant and water were carefully weighed on an analytical balance and mixed. Then, the mixture was stirred at 25  $^{\circ}$ C for 30–60 min until the surfactant became completely dissolved. The experimental characterization of the obtained solutions was made after at least one day storage at ambient temperature (25  $^{\circ}$ C). All L1695 concentrations reported throughout the paper are given in weight percentages relative to the total weight of the obtained solution.

For the samples containing urea, a 6 M (36 wt%) urea solution in water was first prepared and subsequently used to dissolve the desired amount of L1695 surfactant at 25 °C. The aim of these experiments was to determine how replacing part of the water molecules with urea influences interactions between surfactant micelles. To ensure consistency, the solvent composition was kept constant across all experiments by dissolving different L1695 concentrations in the same solvent medium (water  $\pm$  6 M urea). Fixing the urea concentration relative to the total solution would have led to variable urea contents across samples  $\pm$  from 6 M at 1 wt% L1695 to about 10 M at 40 wt% L1695. In the adopted approach, the L1695 concentrations varied between 1 and 40 wt%, corresponding to variation of the urea concentration with respect the whole solution, from 6 M (1 wt% L1695) to 3.6 M (40 wt% L1695), respectively.

## 2.2.2. Rheological measurements

The flow behavior of the prepared solutions was investigated using a rotational rheometer (MCR-302e, Anton Paar GmbH, Austria). The measurements were conducted at a constant temperature of 25 °C using a cone-and-plate geometry with a 40 mm diameter cone, a 1° inclination angle, and a truncation gap of 78  $\mu m$ . The apparent shear viscosity was recorded as a function of the applied shear rate in the 0.1–500 s $^{-1}$  range, applied in a logarithmic progression.

# 2.2.3. Measurements of the micelle sizes

The sizes of the micelles formed in the studied L1695 samples were determined using Zetasizer Nano ZS apparatus (Malvern Instruments). The scattered signal at a 173° angle was recorded and analyzed. The measurements were performed with a laser source operating at 633 nm wavelength at a constant temperature set to 25 °C. Intensity-weighted mean hydrodynamic diameter,  $Z_{\rm ave}$ , and the calculated mean volume diameter ( $d_{\rm vmean}$ ) were used as characteristics of the micelle sizes.

#### 2.2.4. Small angle X-ray scattering (SAXS) analysis

The prepared surfactant solutions were also analyzed with an X-ray scattering system (Xeuss 3.0, Xenocs, Sassenage, France). A CuKα X-ray source operating at a wavelength of 0.154 nm (Xeuss 3.0 UHR Dual source Mo/Cu, Xenocs, Sassenage, France) was used, and the scattered signal was recorded with an Eiger2 4 M detector (Dectris Ltd., Baden Deattwil, Switzerland). The sample-to-detector distance (SDD) was set to 750 mm. Data acquisition time was set to 30 min. Silver behenate was used as a standard to precisely determine the sample-to-detector distance and the coordinates of the beam center on the detector. Samples were enclosed into thin glass capillaries with an outer diameter of 1 mm and wall thickness of 10  $\mu m$  (product of WJM Glass, Germany). The measurements were performed at a constant temperature of 25 °C. The recorded signal was analyzed using XSACT software and corrected for the background scattering using the signal obtained from an identical glass capillary filled with deionized water or with water + urea solution, depending on the solvent in the given sample. The analysis of the reduced SAXS data was performed by the SASView 5.0.6 software. A Levenberg-Marquardt fit optimization method was used. The scattering length densities (SLD) were calculated to be: SLD-core =  $7.34 \times 10^{-6}$  $\mathring{A}^{-2}$  (calculated for dodecane), SLD-solvent = 9.47  $\times$  10<sup>-6</sup>  $\mathring{A}^{-2}$  for the spectra obtained in water and  $\approx 10 \times 10^{-6} \text{ Å}^{-2}$  for the spectra obtained in water-urea mixtures. The SLD for the shell was determined from the best fit, as it depends strongly on the sucrose headgroup hydration degree, thus it should be intermediate between  $14.3 \times 10^{-6} \text{ Å}^{-2}$  (calculated for sucrose) and  $9.47 \times 10^{-6} \text{ Å}^{-2}$  for pure water.

#### 2.2.5. NMR analysis

The NMR study was carried out on a Bruker Avance III HD 500 MHz spectrometer (Rheinstetten, Germany) fitted with a high-resolution broadband probe-head with Z gradient. Experiments were conducted at a temperature of 25 °C. The studied samples were prepared as described in Section 2.2.1 above. 0.5 mL of the prepared sample and 0.1 mL of deuterium oxide (99.8 atom % D, product of Carlo Erba) with TMSP-Na-2,2,3,3-d4 as an internal standard (0 ppm) were mixed before the measurement. Topspin 3.6.5 software package (Bruker, USA) was used for spectrum collection and data analysis.

# 2.3. Molecular dynamics simulations

# 2.3.1. Molecular model

To gain a deeper understanding on the observed L1695 phase behavior, we performed computational molecular dynamics (MD) simulations, using sucrose monolaurate molecules and applying the following workflow: *i*) Single molecules of sucrose monolaurate (SML) and urea were geometrically optimized with the hybrid density functional theory (DFT) functional Becke, 3-parameters, Lee–Yang–Parr (B3LYP) [32,33] and basis set 6–31 G\* defined for the atoms H through Zn [34]; *ii*) The molecules were described with the molecular mechanics force field CHARMM36 [35–37] using its original parameters and partial charges for the atoms; *iii*) The model systems were constructed by randomly placing SML molecules within an orthorhombic simulation box with an edge size of 20 nm along each axis, see Supplementary

three spatial dimensions;  $i\nu$ ) The box was filled with water molecules described by the TIP4P (transferable intermolecular potential with 4 points) model [38];  $\nu$ ) When urea was included in the model, its molecules were added randomly after the placement of the SML molecules, see Supplementary Figure S1B. No background electrolyte was used in the simulations. The compositions of all simulated systems are summarized in Table 1.

Figure S1A. Periodic boundary conditions (PBC) were applied in all

# 2.3.2. Computational protocol

The following computational protocol was employed for all constructed molecular systems: i) energy minimization using the Limitedmemory Broyden-Fletcher-Goldfarb-Shanno optimization algorithm L-BFGS [39]; ii) heating to 298 K in the canonical NVT ensemble, with a constant number of particles, N, constant volume, V, and constant temperature, T, using a velocity-rescaling thermostat [40] with a coupling time of 0.1 ps; iii) relaxation of the system for 1 ns in the isothermal-isobaric (NPT) ensemble at 298 K temperature and 1 bar pressure, controlled with a Berendsen barostat [41] with a coupling time of 0.8 ps; iv) running the production MD simulations for 10 ns in the NPT ensemble and 500 ns in the NVT ensemble, using a 2 fs integration step time. Snapshots of the obtained MD trajectories were saved every 10 ps. The NPT simulations were used to adjust the system density, which was monitored over time; 10 ns were sufficient for equilibration. The densities determined from the MD simulations are in good agreement with the experimentally measured densities of L1695 solutions, see Supplementary Figure S1C. During the equilibration period, the box size decreased slightly from 20 nm down to approximately 19.4 nm.

The leapfrog algorithm [42] was used to integrate the equations of motion during heating, relaxation, and production runs. All hydrogen-containing bonds were constrained: the LINCS [43] algorithm was applied to SML molecules, and SETTLE was used for water molecules [44]. Non-bonded interactions were described by a Lennard-Jones potential, combined with a Coulomb term, with a cutoff set to 12 Å and a switching function initiated at 10 Å. Long-range electrostatic interactions were calculated using the Particle Mesh Ewald (PME) method [45,46] with the same cutoff. The GROMACS 2021.3 software package [47] was used for all simulations and analyses, whereas VMD was employed for visualization of the trajectories [48].

# 2.3.3. Analysis of the MD trajectories

The generated MD trajectories were subjected to the following analyses: i) System density during the initial 10 ns in the NPT ensemble was extracted from the energy file using the default GROMACS tool  $\textit{gmx energy};\ ii)$  Solvent-accessible surface area (SASA), normalized per molecule, was calculated using gmx sasa with the default solvent probe radius of 0.14 nm for water. This analysis provides information about the hydration of molecular fragments within the micelles over the simulation time; iii) Hydrogen bonds (HB) were analyzed using  $\textit{gmx hbond},\$ applying the geometric criteria of a donor-acceptor distance,  $r \leq r_{HB} = 0.35$  nm, and a donor-hydrogen acceptor angle deviation  $\leq 30^\circ$  from the ideal  $180^\circ;\ i\nu)$  Center-of-mass distances between pairs of sucrose headgroups were calculated using gmx dist as a function of time.

**Table 1**Composition of the systems studied by molecular dynamics simulations.

SML concentration, wt%	Concentration, M			Number of molecules			Water-to-SML molecules ratio
	SML	Urea	H <sub>2</sub> O	SML	Urea	H <sub>2</sub> O	
2.5	0.048	0	54	230	0	258 257	1123
	0.048	6.0	35	230	28 900	166 938	726
5	0.095	0	53	415	0	253 094	610
	0.095	6.0	33	460	28 900	161 309	351
16	0.305	0	46	1470	0	223 923	152
	0.305	5.0	28	1470	24 276	136 799	93
40	0.760	0	35	3669	0	167 593	46
	0.760	3.6	24	3669	17 300	117 830	32

The obtained values were processed to obtain distance distribution plots; *v*) Radial distribution functions (RDFs) for specific molecular fragments relative to the geometrical center of selected spherical micelles were computed with *gmx rdf* and normalized to the number density of the molecules within each analyzed micelle to allow comparison; *vi*) Partial density profiles of molecular fragments in the *xy*-plane were obtained using *gmx density*, calculated from the center along the *z*-axis of selected aggregated micelle pairs.

As a reference, additional MD simulations were performed for a single solvated SML molecule to eliminate aggregation effects, both in the absence and in the presence of urea. These simulations were also used to estimate the maximum number of hydrogen bonds that one SML molecule forms with water and urea under full solvation conditions.

#### 3. Results and discussion

# 3.1. Concentration-dependent L1695 arrangement in water – experimental results

We began our study by preparing a series of L1695 solutions in water with concentrations varying between 1 and 40 wt%. Note that all these concentrations are well above the critical micellar concentration for this surfactant, which was previously determined to be about 0.036 wt% at 25 °C [31]. All prepared solutions were completely transparent indicating absence of supramolecular aggregates able to scatter the visible light. Furthermore, the solutions were freely flowing, but with a noticeable difference in their viscous properties. To quantify this difference, viscosity measurements were performed. All solutions were found to exhibit Newtonian behavior, as seen from the data presented in Supplementary Figure S2A. This result is in good agreement with the

results reported previously in Ref. [30] for similar solutions.

Fig. 1A presents the constant viscosities determined in our measurements as a function of the surfactant concentration. As seen from the data, the viscosities of the solutions containing  $\leq 20$  wt% L1695 are relatively low, reaching values of ca. 2 mPa.s at 8 wt%, 5 mPa.s at 16 wt %, and 8 mPa.s at 20 wt% L1695 concentrations. However, further increase of the surfactant concentration leads to much steeper increase in the viscosity which raises to ca. 44 mPa.s at 30 wt%, 140 mPa.s at 35 wt % and 640 mPa.s at 40 wt% L1695. Note that even at 40 wt% the solutions were found to exhibit Newtonian behavior, without any indication for change in the type of the structures formed or appearance of the typical for concentrated samples shear-thinning behavior. Therefore, this significant change in the viscosity could not be attributed to the formation of wormlike micelles.

Next, we continued with experiments, studying the molecular arrangement in the different sucrose ester solutions. First, DLS measurements were performed to characterize the average hydrodynamic diameter of the aggregates present in the studied solutions as a function of the surfactant concentration. The obtained results are presented in Fig. 1B,C and in Supplementary Figure S3. The intensity-weighted mean hydrodynamic diameter,  $Z_{ave}$ , was found to remain relatively constant at concentrations between 2.5 and 8 wt%,  $Z_{ave} \approx 5.4 \pm 0.3$  nm. However, at 1 wt% concentration, it was slightly lower  $Z_{ave} \approx 4.3 \pm 0.2$  nm, whereas at concentrations exceeding 10 wt% the measured values increased significantly. Note that the 1 nm difference between the sizes measured for 1 wt% sample and that for 2.5 – 8 wt% samples, already indicates a possible interaction between the L1695 micelles even at low surfactant concentrations of only few percent.

The significant increase of the sizes detected for solutions containing 12 and 16 wt% L1695 did not change the micelles size distribution by

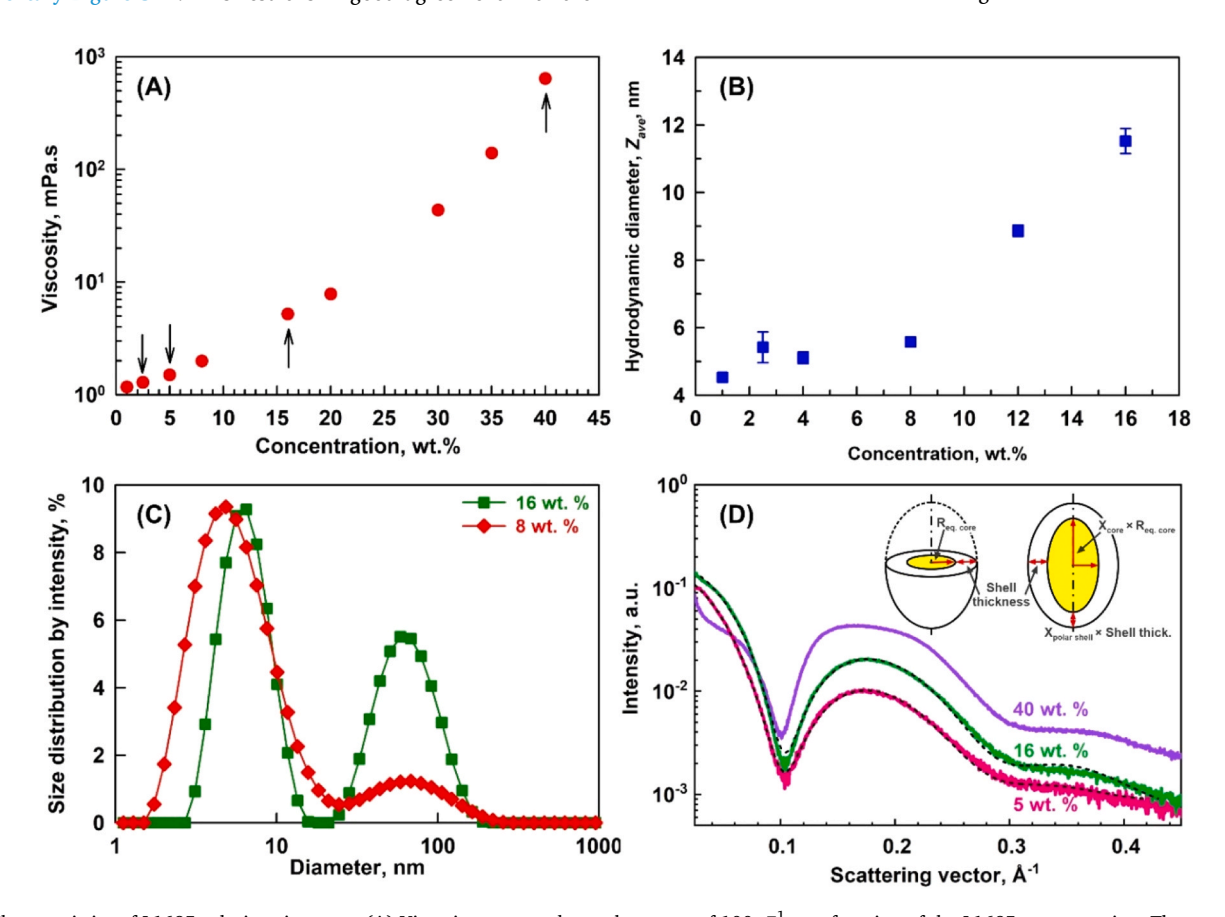


**Fig. 1.** Characteristics of L1695 solutions in water. (A) Viscosity measured at a shear rate of 100 s<sup>-1</sup> as a function of the L1695 concentration. The arrows denote concentrations at which MD simulations were performed. (B,C) Hydrodynamic diameter (B) and intensity-weighted size distributions (C) measured by DLS. (D) SAXS curves obtained for 5 wt% (magenta), 16 wt% (green) and 40 wt% (purple) L1695 solutions. Curves are not shifted with respect to the y-axis. The black dashed lines represent the theoretical fits of the curves, see text for more details. Inset: parameters used in the core-shell ellipsoid model applied for the SAXS spectra description.

volume. It remained with a single almost Gaussian-shaped peak even at 16 wt%, see Supplementary Figure S3B. The peak maximum shifted to slightly higher diameters. Much bigger differences were observed in the intensity-weighted size distributions, which are known to be more sensitive to the presence of larger particles (as the scattering intensity is proportional to the sixth power of the object diameter [49]), see Fig. 1C. A main peak centered between 4 and 6.5 nm was present in all samples (its position increased slightly with the increase of the surfactant concentration). However, a second peak with a maximum around 60 nm was also present in all samples. The intensity of this second peak increased significantly with the increase of the L1695 concentration, see Fig. 1C. These results show that aggregates bigger than the individual spherical micelles are present in the L1695 solutions even at 1 wt% concentration, see Supplementary Figure S3A. The size and number of these aggregates increases significantly with the increase of the surfactant concentration.

To further characterize the shape and size of these aggregates, next we conducted X-ray scattering experiments. Illustrative curves showing the typical SAXS curves obtained depending on the L1695 concentrations are presented in Fig. 1D. As seen, for all studied samples a wide peak with a maximum at ca. 0.17  $\mbox{\sc A}^{-1}$  is observed. The intensity of this peak increased significantly with the increase of the surfactant concentration, while its width broadened.

The obtained spectra were described theoretically using the SASView software to extract detailed information about the structure, size and shape of the particles present in the investigated samples. A core-shell model was chosen, as typically used for surfactant micelles [50]. However, modelling micelles as spheres resulted in relatively big fitting errors, leading us to adopt the core-shell ellipsoid model. Note that the SAXS spectra clearly indicate the presence of non-spherical objects. If the micelles were spherical, the slope of the scattering intensity versus the scattering vector, q, at low q-values would be expected to approach zero, which is not observed in the obtained spectra.

In the adopted approach the scattering entities are described by four main parameters, see the inset in Fig. 1D. These are: two radii of the core (equatorial radius  $R_{eq.core}$  and polar radius  $R_{eq.core} \times x_{core},$  which includes the core axial ratio  $x_{\text{core}}\!)$  and two shell thicknesses (equatorial Shell thickness and the polar shell thickness, defined as shell thickness  $\times$  $x_{polar \; shell}$ , where the parameter  $x_{polar \; shell}$  accounts for asymmetry in the shell thickness along the ellipsoid polar axis). Since the currently studied micelles were expected to have a uniform shell structure,  $x_{polar\ shell}$  was initially fixed at 1. The shell SLD value was set to  $11.3 \times 10^{-6} \text{ Å}^{-2}$ , as initially fitting results indicated that values near this yielded the best agreement with the experimental data. This choice was later supported by the results obtained from the MD simulations, see Section 3.4 below. This SLD value represents an average scattering length density, accounting for contributions from sucrose, water molecules which hydrates it, and the terminal methylene groups of the hydrophobic tail to which the headgroup is attached.

Using the core-shell ellipsoid model under the assumption that the ellipsoid shell thickness is uniform (i.e.  $x_{polar\ shell}=1$ ) yielded unsatisfactory fits (fitting error  $\chi^2=4.40$ ) even for the most diluted samples studied with 5 wt% L1695, see Supplementary Figure S4. Relaxing this assumption led to significantly improved fit, for  $x_{polar\ shell}=0.45$  the fitting error became  $\chi^2=0.73$ , see Supplementary Table S1.

Notably, when varying the values of the  $x_{polar\ shell}$ , the values of the equatorial radius and the shell thicknesses remained relatively constant,  $R_{eq.core} \approx 12.9 \pm 0.3$  Å, and the shell thickness  $\approx 13.7 \pm 0.5$  Å. According to the model, the equatorial size of the micelles is equal to the doubled sum of  $R_{eq.core}$  and shell thickness, which is  $\approx 5.3$  nm. This size is in excellent agreement with the average hydrodynamic diameter measured in the DLS experiments ( $Z_{ave} \approx 5.4 \pm 0.3$  nm).

Variations in the  $x_{polar\ shell}$  parameter led to modest changes in the  $x_{core}$  value, which practically defines the aspect ratio of the ellipsoids. Depending on the value of  $x_{polar\ shell}$ ,  $x_{core}$  ranged between ca. 3.5 and 5. For  $x_{polar\ shell}=0.31$ , where the best fit was achieved,  $x_{core}\approx 4.3$ . These

values indicate that the micelles are likely elongated. However, this conclusion is contradicted by rheological data. In systems with elongated micelles, increasing surfactant concentration typically leads to the formation of wormlike micelles, which would result in non-Newtonian behavior. In contrast, the L1695 solutions retained their Newtonian viscoelastic properties even at 40 wt% L1695, suggesting that an alternative explanation is required.

The SAXS results obtained with 16 wt% L1695 in water were successfully described ( $\chi^2 = 2.09$ ) using the same core-shell ellipsoid model and similar experimental parameters, see the solid line in Fig. 1D. Specifically,  $R_{eq.core} \approx 13.3$  Å, shell thickness  $\approx 12.0$  Å,  $x_{polar\ shell} \approx 0.64$ , and  $x_{core} \approx 2.55$ , see also Fig. 6C below which summarizes the fit parameters obtained at different concentrations. Polydispersity for the Rea. core was introduced in the model, with a Gaussian function, and polydispersity was calculated to be equal to 0.06. Using the obtained results and the core-shell ellipsoid geometry, we estimate that the volume ratio between the tails and heads in the micelles is  $V_{tails}/V_{heads} \approx 0.29$ . This corresponds to an average SLD for the entire L1695 molecule of approximately  $10.15 \times 10^{-6} \text{ Å}^{-2}$ , taking into account the individual SLDs of the shell and core used in the data fitting. This value agrees well with the SLD derived independently from density measurements. For a 16 wt% L1695 solution, we measured a density of  $\rho \approx 1010 \pm 5 \text{ kg.m}^{-3}$ at 25°C, Supplementary Figure S1C, which indicates that the density of the hydrated L1695 molecules in this solution is  $1084 \pm 35 \text{ kg.m}^{-3}$ . Using the molecular mass of sucrose monolaurate (524.6 g.mol<sup>-1</sup>) and The close agreement between the two SLD values supports the SAXS data analysis.

However, a model without a structure factor failed to appropriately describe the scattering data from the 40 wt% samples. In this case, the estimated L1695 density, based on the bulk solution density, was 1189  $\pm$  15 kg.m $^{-3}$ , indicating significant decrease in surfactant hydration. To determine what would be the appropriate model to describe these data and gain further insight into the structural arrangement of sucrose monolaurate molecules in water, next we performed molecular dynamics simulations. The interpretation of the SAXS results is further discussed in Section 3.3 below.

# 3.2. Sucrose monolaurate arrangement in water – molecular dynamics simulations

Atomistic molecular dynamics simulations were performed to further investigate the arrangement of sucrose monolaurate molecules at four different concentrations – 2.5, 5, 16 and 40 wt%. Snapshots of the molecular configurations obtained after 500 ns simulation time are shown in Fig. 2. At the lowest simulated concentration, small spherical micelles were formed. Two of the micelles remained as individual entities in the simulation box, while the other three aggregated by the end of the simulation. Although aggregation proceeded after ca. 350 ns of simulation, the micelles did not fully merge even after 150 ns of contact with one another. They remained aggregated due to the interactions between their sucrose heads.

Increasing the surfactant concentration to 5 wt% led to more pronounced aggregation. In this simulation, all small micelles assembled into a single larger aggregate. Much bigger aggregates with irregular and branched thread-like structures were formed at the higher concentrations studied, 16 wt% and 40 wt%. Nevertheless, the primary micelles retained their distinct identities, without any sign of complete merging or the formation of wormlike micelles, see Fig. 2.

The analysis of the clustering process, see Supplementary Figure S5, shows that the average size of the clusters increases gradually up to 300 ns and reaches a plateau afterwards. This further confirms that initially the primary spherical micelles form, which then further aggregate due to the interactions between the hydrophilic sucrose headgroups present on the micelles surface. The primary micelles were found to have an aggregation number varying between 60 and 100.

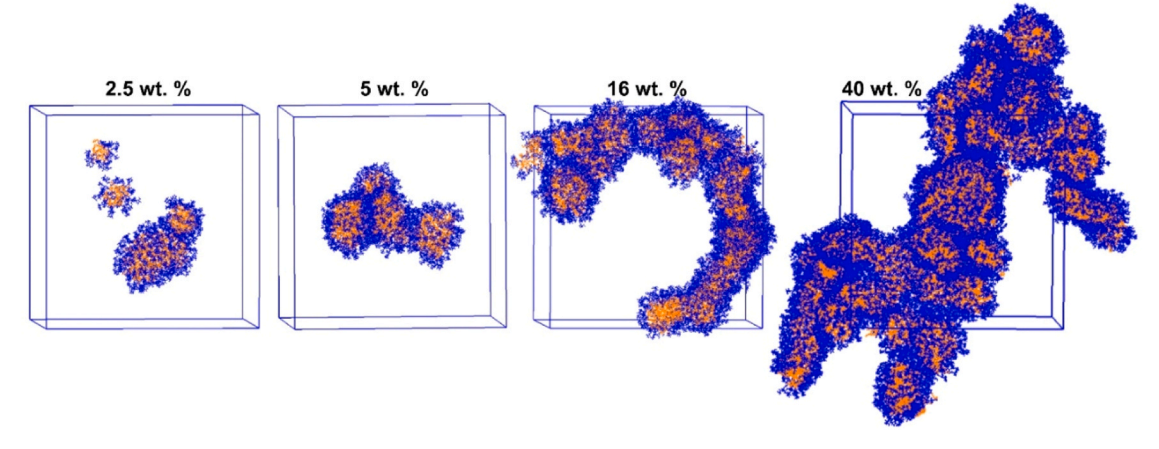


Fig. 2. Snapshots of the SML molecular configurations at various concentrations after 500 ns of atomistic MD simulations. Alkyl tails are shown in orange and sucrose headgroups in blue.

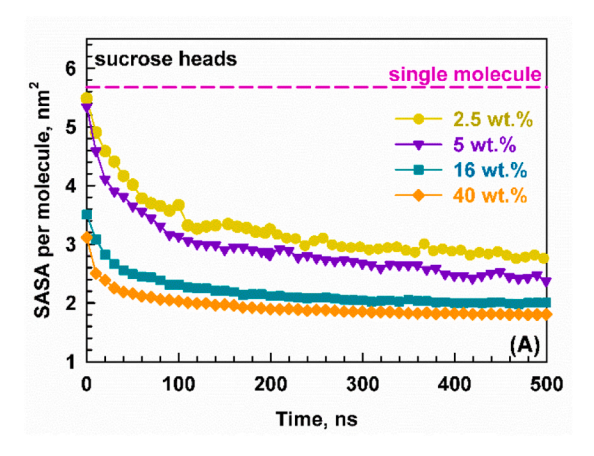
Their formation is analyzed and discussed in more details in Section 3.4 below, where the effect of hydrogen-bonds disrupting additive, urea, is also described.

To investigate the aggregation behavior of SML molecules, we analyzed the concentration-dependent evolution of the solventaccessible surface area (SASA) over time for both the sucrose headgroups and the alkyl tails, see Fig. 3. As a reference, an additional MD simulation with a single solvated SML molecule was performed to eliminate the effects of molecular aggregation. From this simulation, we obtained SASA values of approximately 5.7 nm<sup>2</sup> for the sucrose headgroup and 4.2 nm<sup>2</sup> for the lauric alkyl tail. Both of these areas were found to decrease significantly upon increase of the SML concentration in the simulations, see Fig. 3. In particular, the initial SASA values determined at the lower investigated concentrations (2.5 and 5 wt%) were similar to those for the single molecule. However, the SASA of the sucrose headgroups decreased exponentially over time, reaching approximately 2.8 nm<sup>2</sup> and 2.5 nm<sup>2</sup> after 500 ns for surfactant concentrations of 2.5 and 5 wt%, respectively, Fig. 3A. Additional 200 ns simulations were performed for the 2.5 wt% system to check whether the SASA will decrease further, but the observed decrease was relatively small (< 10 %).

Even faster decrease in the SASA values was observed for the sucrose headgroups in the simulations performed at higher (> 5 wt%) SML concentrations. In these cases, the initial SASA values were already significantly lower - 3.5 and 3.1 nm $^2$  for the 16 wt% and 40 wt% systems, respectively. These values decreased to 2.0 and 1.8 nm $^2$  at the end

of the simulations. The notably lower initial SASA values for the hydrophilic headgroups at higher SML concentrations can be attributed to the substantially reduced water content in these systems compared to those with lower surfactant concentrations. For instance, the water-to-SML molecule ratio is approximately 1123 in the 2.5 wt% simulation, whereas it decreases to 152 and 45.7 in the 16 wt% and 40 wt% systems, respectively, see Table 1. Therefore, while the randomly distributed SML molecules in the low concentration simulations are initially fully hydrated due to the abundant water, those in the more concentrated systems have already lost part of their hydration capacity at the start of the simulations due to their close contact with other SML molecules. Consequently, the SASA values for the high-concentration systems decreased by ca. 5 % between the 200 ns and 500 ns, whereas about 15 % decrease in the SASA values was observed for the 2.5 and 5 wt% SML systems.

The differences observed in the SASA values for the hydrophilic headgroups at different SML concentrations diminished when the SASA values of the alkyl tails were analyzed, see Fig. 3B. The initial SASA values were again similar to those of individual SML molecules at low concentrations and significantly lower at higher SML concentrations. However, all simulations showed a rapid SASA decrease, reaching a similar final area of approximately 1.0 nm², independently of the studied surfactant concentration. The time required to reach this value was ca. 50 ns for the concentrated systems and about 150 ns for the more diluted ones. This constant value shows that, even at lower concentrations, the micelles formed have a well-defined hydrophobic core,



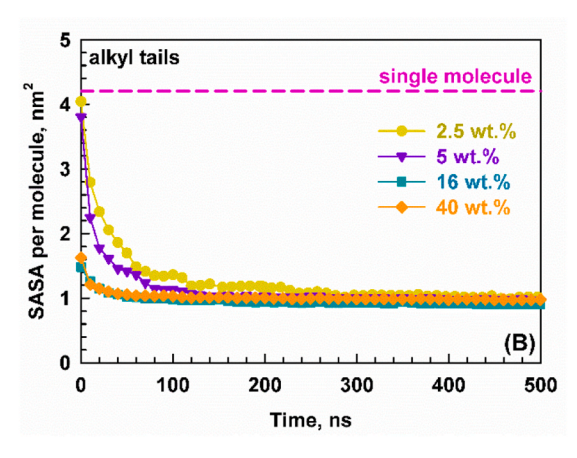


Fig. 3. Solvent-accessible surface area (SASA) per molecule as a function of time. (A) SASA of the sucrose headgroup. (B) SASA of the alkyl tails. Different colors indicate the SML concentrations used in the simulations: 2.5 wt% (yellow circles), 5 wt% (purple reversed triangles), 16 wt% (cyan squares), and 40 wt% (orange diamonds). Dashed pink lines represent reference values obtained from simulations of a single SML molecule.

which is relatively inaccessible to the water molecules.

The reduced SASA values observed for the hydrophilic headgroups at higher surfactant concentrations indicate a decrease in the headgroup hydration as larger aggregates form through the association of the primary spherical micelles. This likely occurs due to a reduction in the interactions between the surfactant headgroups and water, i.e. water molecules surrounding the hydrophilic headgroups are displaced, in favor of increased interaction between the sucrose headgroups themselves. This conclusion is further supported by the increase in the density of L1695 molecules with increasing surfactant concentration.

To investigate this further, we analyzed the number of intermolecular hydrogen bonds formed between sucrose headgroups, as well as those formed between sucrose and water molecules as a function of time. Note that the sucrose monolaurate headgroup contains eight hydroxyl groups, as well as two oxygen atoms connected via ether bonds located within the fructofuranosyl and glucopyranosyl rings. Additionally, two more oxygen atoms are present in the ester bond through which the hydrophobic tail is attached. In total, the SML structure contains 12 oxygen atoms, all of which can act as hydrogen acceptors. Furthermore, there are 7 hydrogen atoms which can participate in hydrogen bonds, as they are bound to an electronegative atom, making a maximum possible number of 19 hydrogen bonds per molecule.

Fig. 4 shows the evolution of the number of hydrogen bonds over time. Similar to the trends observed in the SASA analysis, the systems at the lower concentrations, 2.5 and 5 wt% SML exhibited comparable behavior, as did those at the higher concentrations – 16 and 40 wt% SML. The analysis of the hydrogen bonds formed between the sucrose headgroups and water molecules revealed a significant decrease over time, see Fig. 4A. At low SML concentrations, the number of hydrogen bonds began at ca. 13 and decreased down to 8–9 after 500 ns. At higher concentrations, the initial number was around 9–10 and it dropped down to ca. 7 by the end of the simulations. These results show that both increase of the surfactant concentration and molecular rearrangement upon relaxation reduce the number of hydrogen bonds formed between SML molecules and water.

In contrast, the number of intermolecular hydrogen bonds formed between the sucrose headgroups of the individual SML molecules was found to increase with the increase of the surfactant concentration, Fig. 4B. Specifically, no intermolecular hydrogen bonds were initially observed for the 2.5 and 5 wt% SML simulations. However, upon micellization the average number of intermolecular hydrogen bonds formed by each SML molecule increased to approximately 1.3 for 2.5 wt% SML and 1.5 for 5 wt% SML systems.

At the higher concentrations studied, one intermolecular sucrosesucrose hydrogen bond was present at the start of the simulation, and an additional bond formed upon aggregation. We note that the number of intermolecular hydrogen bonds was determined by first calculating the total number of hydrogen bonds between sucrose headgroups across all molecules in the simulation. This total was divided by the number of SML molecules in the simulation and then 1.5 was subtracted from the obtained number to account for intramolecular bonds formed within a given molecule. This reference value was obtained from a separate analysis of the simulation with a single SML molecule, as well as from the analysis of the number of hydrogen bonds formed by each individual SML molecule in the 2.5 wt% simulation, see Supplementary Figure S6 showing the probability distribution obtained from this analysis.

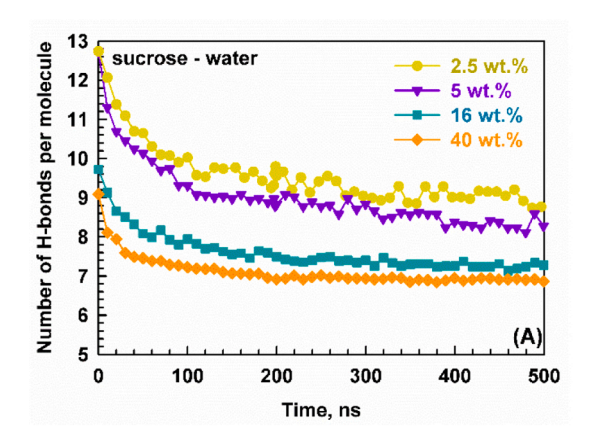
The results from the hydrogen bonds analysis strongly suggest that the formation of hydrogen bonds between the sucrose headgroups is driving the SML assembly in larger aggregates, composed of primary micelles. These intermolecular sucrose-sucrose hydrogen bonds form at the expense of hydrogen bonds with water molecules (part of which break), which probably contributes to the higher viscosity of the solutions observed upon increase of the SML concentration. Notably, the primary micelles do not merge together but maintain their individuality within the larger aggregates, thus resembling closely packed "pearl necklace" arrangement which is known for polymers [51].

These findings agree with the results obtained from the SAXS analysis as well, where the micelle aspect ratio, determined by the  $x_{core}$  parameter, was found to be greater than 1. This value reflects the average number of micelles that have aggregated together, or at least the average size of the segment within the larger aggregates which is distinguishable by X-ray contrast, as the shells of individual micelles are partially fused ( $x_{polar}$  shell is between 0.45 and 0.78).

To further investigate the role of hydrogen bonding between individual sucrose laurate molecules, we performed additional experiments in the presence of urea, which is known to act as an efficient hydrogen bond disrupting agent [52–55]. The results from these experiments and molecular dynamics simulations are presented in the following sections.

## 3.3. Effect of urea on the aggregation behavior of L1695

Urea, a strong hydrogen bond donor, has been widely recognized as a denaturing osmolyte for proteins, shifting the equilibrium between the unfolded and folded states towards the unfolded ones [52]. The mechanism behind this action has been widely debated but it has been established that the main urea action is related to the disruption of the intermolecular hydrogen bonds in expense for the formation of stronger intermolecular hydrogen bonds between the urea and the protein backbone [52–54]. Furthermore, urea has been shown to impact also the critical micellar concentration (CMC) of both ionic and nonionic surfactants [55–59]. For nonionic surfactants, an increase in the CMC values has been observed, which is explained with the ability of urea to



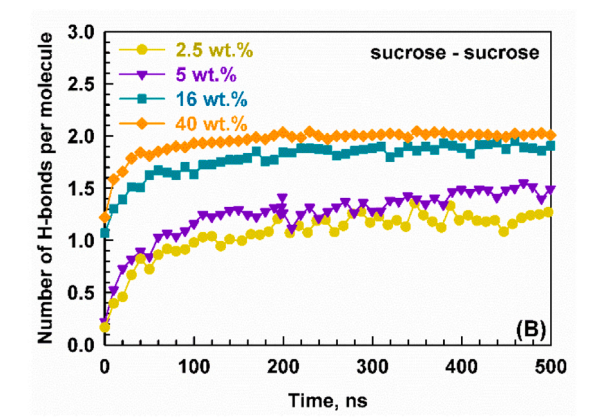


Fig. 4. Number of hydrogens bonds formed per one sucrose laurate molecule between: (A) Sucrose heads and water; (B) Sucrose headgroups from different molecules. Different colors indicate the SML concentrations used in the simulations: 2.5 wt% (yellow circles), 5 wt% (purple reversed triangles), 16 wt% (cyan squares), and 40 wt% (orange diamonds).

displace the water molecules from the hydration shell.

To study the effect of urea addition over the aggregation behavior observed for the L1695 surfactant, we prepared samples containing 6 M urea with respect to the water and investigated their properties. The rheology measurements of the samples containing urea showed Newtonian behavior for all studied surfactant concentrations, up to 40 wt% L1695, see Supplementary Figure S2B.

To be able to compare the surfactant solutions viscosities excluding the contribution from the viscosity of the phase in which the surfactant has been dissolved, we calculated the relative viscosities of the samples by dividing the measured viscosity in the presence of surfactant by the viscosity of the solvent used, i.e. 0.89 mPa.s for water and 1.5 mPa.s for the 6 M aqueous urea solution (see Supplementary Figure S2B). Then, the ratio between the relative viscosity calculated for the pure water samples and the one for samples prepared in the presence of urea was taken. The obtained data are presented in Fig. 5A. As seen from the graph, even for the 5 wt% L1695 sample, the calculated ratio, ( $\eta_{surf}$ /  $\eta_{H2O})$  /  $(\eta_{surf\text{-}urea}/\eta_{H2O\text{-}urea})$  is  $\approx 1.4 > 1.$  This shows that the relative viscosity of the aqueous solution without urea is higher than that of the solution prepared with urea. Remarkably, increase of the surfactant concentration to 16 and 40 wt% yielded significantly higher relative viscosity ratios  $\approx$  6–7. This substantial reduction in the viscosities of solutions containing urea can be attributed to interaction between urea and the surfactant molecules, which likely disrupt part of the intermolecular hydrogen bonds and alter the structural arrangement present in urea-free solutions. This conclusion was further confirmed by the results obtained from the molecular dynamics simulations, see Section 3.4 below.

DLS analysis revealed a pronounced reduction in large aggregates in samples containing urea, accompanied by a marked increase in the intensity of the 6.5 nm peak in 16 wt% samples, see Fig. 5B. Two distinct size populations were observed in all samples: micelles centered at

6.5 nm, whose relative abundance increased from 10 % to 14 % upon urea addition in the 16 wt% L1695 sample, and a second population corresponding to larger aggregates. The latter peak was centered around 60 nm in solutions without urea and shifted to approximately 200 nm in the presence of urea, while its amplitude decreased significantly from 2.7 % to 0.7 % (for 16 wt% samples). This result indicates that aggregates formed in the absence of urea are more compact due to the higher number of inter-micellar hydrogen bonds. In contrast, the addition of urea leads to its adsorption on the micelle surface. This prevents the strong inter-micellar interactions, leading to the formation of larger but less cohesive aggregates. Similar trends were observed across all studied concentrations, see Supplementary Figure S7.

The impact of urea on the molecular packing of L1695 molecules was further evident from the diffusion-ordered spectroscopy (DOSY) NMR data, see Fig. 5C. The data demonstrate a clear difference in the self-diffusion coefficients of 16 wt% L1695 samples measured in the presence and absence of urea. In pure water, the average diffusion coefficient was approximately 32  $\mu m^2.s^{-1}$ , whereas for the urea-containing sample it increased to 50  $\mu m^2.s^{-1}$ . This result directly demonstrates the significantly increased mobility of surfactant molecules in the samples containing urea compared to those without, confirming that urea effectively disrupts the extended micellar network and reduces the hydrodynamic volume of the diffusing aggregates.

The obtained self-diffusion coefficients were further used to calculate the average size of the micelles present in the solutions with and without urea. This was done using the Stokes-Einstein equation [60]:

$$d_H = \frac{k_B T}{3\pi \eta D} \tag{1}$$

where  $d_{\rm H}$  is the hydrodynamic diameter of the diffusing particles,  $k_{\rm B}$  is the Boltzmann constant (1.38 ×10<sup>-23</sup> J.K<sup>-1</sup>), T is the temperature

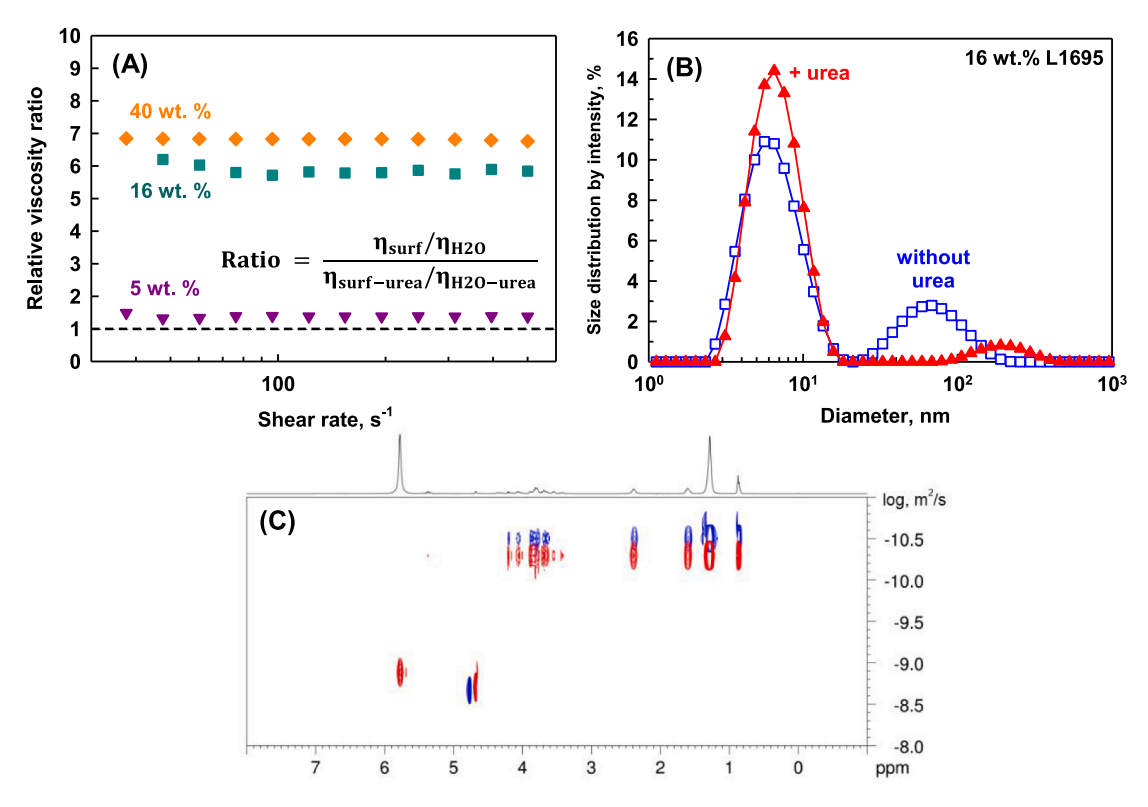


Fig. 5. Effect of urea on the properties of L1695 solutions. (A) Relative viscosity ratio for 5 wt% L1695 (purple reversed triangles), 16 wt% L1695 (cyan squares) and 40 wt% (orange diamonds) samples. The presented data were calculated by taking the ratio of the viscosity of the surfactant solution in water ( $\eta_{surf-urea}$ ) relative to the viscosity of the pure ureawater mixture ( $\eta_{H2O-urea}$ ). (B) Size distribution measured by intensity for 16 wt% L1695 solution with (filled red triangles) and without (empty blue squares) 6 M urea in the aqueous phase. (C) DOSY NMR-spectra for 16 wt% L1695 solution in water (blue) and in the presence of 6 M urea (red).

(298.15 K in the present case),  $\eta$  is the viscosity of the media through which the particles are diffusing, and D is the measured self-diffusion coefficient. Assuming that the micelles present in the solutions have spherical shape (as also confirmed by the results from the molecular dynamics simulations), values of  $d_H \approx 5.8$  nm in presence of urea and 15.3 nm in absence of urea were calculated. For these estimates, viscosities of 1.5 mPa.s and 0.89 mPa.s were used for the urea-containing sample and for the sample prepared without urea, respectively. This result is in good agreement with the findings from the DLS analysis, suggesting that the number of large aggregates in the sample decreases significantly when urea is added.

Similar conclusions were drawn from the analysis of the SAXS results, see Fig. 6. The spectra for 16 wt% samples obtained in water and in 6 M urea were successfully described using a core-shell ellipsoid model. The  $x_{core}$  parameter decreased for the sample prepared in urea as compared to that in water, demonstrating the decreased connectivity of the individual micelles. This conclusion was further supported by the results obtained from the 40 wt% samples, where  $x_{core} \approx 1.9$  for the sample in water and  $x_{core} \approx 1.4$  for the sample in 6 M urea. Furthermore,

the theoretical description of the scattering spectra obtained for 40 wt% samples became only possible when a structure factor was included in the model.

Considering the results from the molecular dynamics simulations, we chose to use the "sticky" hard sphere structure factor with Percus-Yevick closure [61–63]. In this model, the individual particles are considered to interact with one another via short-range attractive forces. The structure factor is described by four additional parameters: the effective radius of the spheres, which was set to be equal to the average outer radius; the volume fraction of the hard spheres; the perturbation parameter, which practically defines the length scale at which the individual spheres interact with one another (it was set to 0.012), and the stickiness parameter,  $\epsilon$ , which shows the attraction interaction strength. Smaller values of  $\epsilon$  correspond to stronger attraction. Accordingly, the stickiness parameter was found to be  $\epsilon \approx 0.5$  for the 40 wt% L1695 sample in water, whereas it increased significantly when the same surfactant concentration was investigated in water-urea mixture,  $\epsilon \approx 24.2$ .

We note that although the arrangement observed in the MD simulations resembled a closely-packed "pearl necklace", the classical "pearl

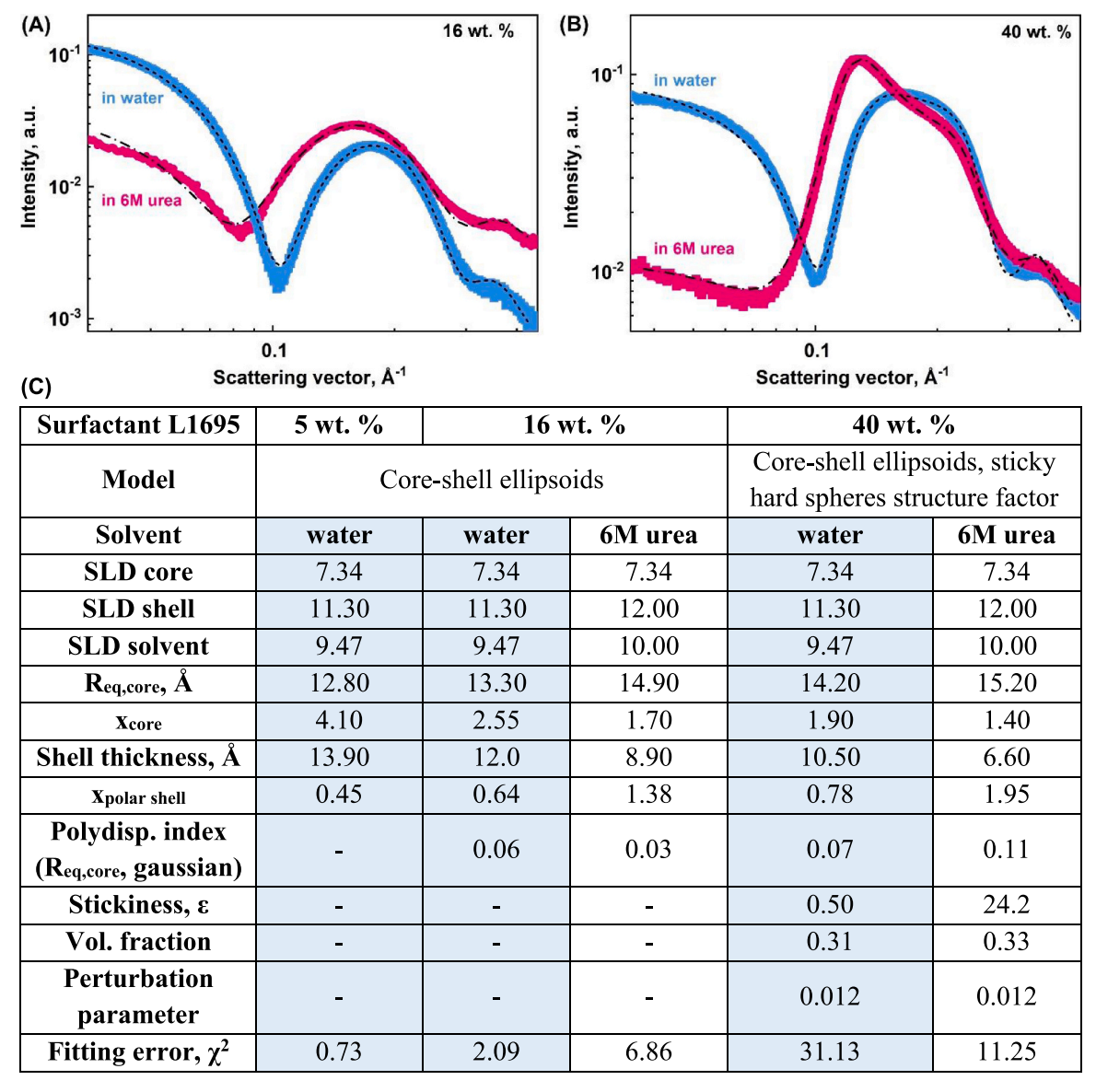


Fig. 6. (A,B) SAXS spectra obtained from: (A) 16 wt% L1695 and (B) 40 wt% L1695 samples in water (blue symbols) and in 6 M urea (purple symbols). (C) Parameters obtained from the SAXS spectra fitted using core-shell ellipsoid model. The fits are plotted in (A,B) with dashed curves for the samples dissolved in water, and with dashed-dot curves for the samples dissolved in 6 M urea. Data for 5 wt% curve plotted in Fig. 1D are also included.

| | "

necklace" model assumes homogeneous pearls connected by a string with its own scattering length density and a defined chain linkage length. These assumptions are not met in the present system, where the micelles have a core-shell structure and aggregate via inter-micellar hydrogen bonds, making the model inapplicable. Nevertheless, the use of a sticky hard sphere structure factor to describe the scattering profiles at higher surfactant concentrations supports the proposed structure, which is also directly observed in the MD simulations. Including the sticky hard sphere structure factor allowed the SAXS spectra to be fitted even with the core-shell spheres model rather than core-shell ellipsoids. However, the fitting error in this case was significantly higher, likely because the micelles in the aggregates are not identical in size, and their partial fusion varies along the thread-like structures, reducing the X-ray contrast.

All these results suggest that urea significantly affects the self-assembly behavior of the surfactant molecules. The reduction in viscosity and the shift in size distribution indicate that urea disrupts intermolecular interactions, possibly by weakening hydrogen bonding or altering hydration layers around the surfactant molecules. Consequently, the presence of urea leads to smaller, less organized aggregates and a more fluid-like behavior, which could have implications for formulation design in surfactant-based systems. To obtain further insights about the urea effect over the sucrose monolaurate self-assembly, next we compare the results from the molecular dynamics simulations performed in presence and in absence of urea.

# 3.4. Aggregation behavior of SML in presence of urea studied by MD simulations

To assess the behavior of a sucrose monolaurate molecule in the absence of intermolecular interactions between the sucrose heads, we first simulated a reference system containing a single SML molecule placed in a water-urea solution. The urea concentration was set to 6 M compared to the water to be the same as in the actual experiments. The results obtained from this simulation are compared to these of the simulation performed in absence of urea in Table 2. The solventaccessible surface area (SASA) was found to remain practically the same in presence and in absence of urea,  $SASA_{heads} \approx 5.66 \pm 0.02 \text{ nm}^2$ and SASA<sub>tails</sub>  $\approx 4.20 \pm 0.01 \text{ nm}^2$ . This result is expected as a single SML molecule analyzed in the presence of urea is not expected to change its conformation. However, a significant difference was observed in the number of intermolecular hydrogen bonds formed between the SML and water. While the SML molecule formed about 13 hydrogen bonds in pure water, this number decreased down to 9 upon the addition of urea. The four disrupted hydrogen bonds were replaced by new ones formed between the SML molecule and urea. The number of the intramolecular hydrogen bonds remained unchanged at approximately 1.45  $\pm$  0.05.

Next, MD simulations were performed at different SML concentrations and urea molecules randomly distributed among the surfactant monomers. A snapshot of the molecular assembly after 500 ns simulation at 16 wt% SML is shown in Fig. 7A. The resulting structure differs significantly from that shown in Fig. 2, which depicts the system without urea. While the addition of urea did not completely suppress micelles aggregation, it significantly altered their organization. Instead of forming a single, interconnected, thread-like structure, the SML micelles preserved to much higher extent their individuality when urea was present. The resulting assembly has reduced connectivity and increased porosity, with some micelles remaining as distinct entities within the urea-water solution. This structural breakdown is consistent with the well-known ability of urea to interfere with hydrogen bonding and alter solvation structures, thereby weakening the intermolecular interactions responsible for the supramolecular organization. Furthermore, the obtained picture is also in good agreement with the experimental results showing that urea disrupts structured assemblies of sucrose laurate and promotes a transition toward a more fluid, less entangled state.

To gain a deeper insight into the dynamics and stability of aggregate

Average values for solvent-accessible surface area (SASA) and number of hydrogen bonds calculated from the molecular dynamic simulations

		6			•						
SML concentration		Single molecule	cule	2.5 wt%		5 wt%		16 wt%		40 wt%	
Solvent		$H_2O$	$H_2O + urea$	$H_2O$	$H_2O + wrea$	$H_2O$	$H_2O + urea$	$H_2O$	$H_2O + wrea$	H <sub>2</sub> 0	$H_2O + urea$
SASA, nm <sup>2</sup>	heads	5.68	5.65	2.74	4.01	2.46	3.56	2.00	3.00	1.81	2.47
	tails	4.21	4.20	1.02	1.48	96.0	1.20	0.91	1.06	86.0	96.0
Average number of H-bonds per molecule Intramolecular sucrose-sucrose	Intramolecular sucrose-sucrose	$1.4\pm0.7$	$1.5\pm0.7$	$1.2\pm0.8$	$1.4\pm0.8$	,					
(300-500 ns)	Intermolecular sucrose-sucrose			$1.4\pm0.1$	0.5	$1.6\pm0.1$	0.7	$2.0\pm0.1$	$2.0 \pm 0.1$ $1.0 \pm 0.1$	$2.0\pm0.1$	1.3
	$(-1.36 \text{ for H}_20)$										
	$-1.5$ for urea $+$ $\mathrm{H}_2\mathrm{O}$										
	Intermolecular sucrose-water	$13.2\pm1.9$	$9.4\pm2.2$	$9.0\pm0.2$	$7.7\pm0.2$	$8.5 \pm 0.2$	$7.2\pm0.1$	$7.3\pm0.1$	$6.8\pm0.1$	$6.9\pm0.1$	$6.4\pm0.1$
	Intermolecular sucrose-urea		$4.1\pm2.1$		3.6		3.4		3.1		2.5
	Total number intermolecular	13.2	13.5	10.4	11.8	10.1	11.3	9.3	10.9	6.8	10.2

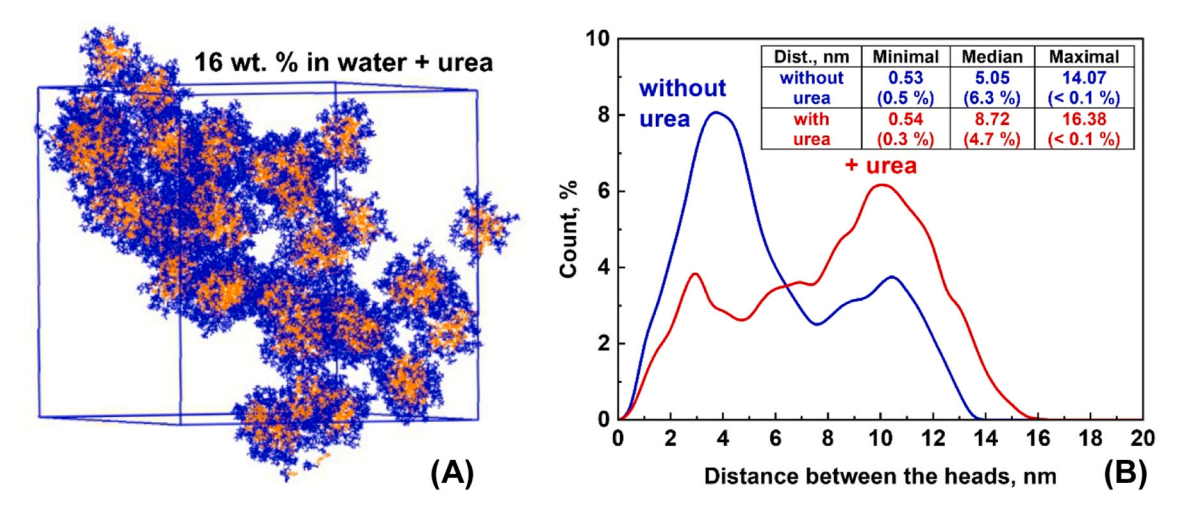


Fig. 7. (A) Molecular arrangement at 16 wt% SML after 500 ns of simulation in water-urea medium. (B) Distances between the centers of mass of sucrose head pairs over 400–500 ns at 2.5 wt% SML in the absence (blue line) and presence (red line) of urea. Numbers in brackets indicate the percentage of occurrences of each distance during the analyzed period.

formation, we analyzed the evolution of cluster formation, see Supplementary Figure S8. In pure water, the system exhibits faster aggregation, reaching a constant aggregation number relatively quickly. The specific time required depended on the surfactant concentration. This aggregation process led to the formation of large, stable supramolecular structures. For the 2.5 wt% system, four micelles were observed, each with an average aggregation number of ca. 60, whereas at 16 wt% SML, all micelles aggregated into a single thread-like structure containing nearly all 1470 SML molecules included in the simulation. In contrast, the presence of urea induces markedly different behavior. The average cluster size remains relatively small (ca. 25-35 at 2.5 wt% SML and around 200-500 at 16 wt% SML) and fluctuates around these values throughout the simulation. This indicates that urea significantly hinders interactions between individual SML micelles and suppresses the growth of supra-micellar aggregates. This effect is most probably related to the disruption of hydrogen bonding and alteration in solvent-surfactant interactions.

Quantitatively, these findings are also supported by the SASA and hydrogen bonds analyses, see Table 2 and Supplementary Figures S9 and S10. For example, the SASA for the sucrose heads showed an increase with about 50 % when calculated for the 2.5–16 wt% SML simulations in presence of urea as compared to the values obtained in pure water. The effect for the SASA of the hydrophobic tails was much smaller, but once again the values obtained in presence of urea were slightly higher than those in absence of it, Table 2.

The values for the SASA were obtained by averaging the results between 400 and 500 ns at each SML concentration. For the number of H-bonds, the averaging was done on data obtained from 300 to 500 ns. The errors presented in the table represent the standard deviations of the averaged values. No errors are reported for the SASA values, as they were consistently within  $\pm\,1$ % of the value of the respective quantity. Graphs showing the evolution, i.e. the kinetics, of the reported quantities are available as Supplementary Figures S9 and S10.

The increase of the hydrophilic headgroups exposure to water in presence of urea is mainly due to the decreased intermolecular interactions between the sucrose headgroups which were disrupted due to the presence of urea. The analysis of the average number of hydrogen bonds formed by each surfactant molecule showed that about 2.5-3.6 intermolecular hydrogen bonds between sucrose headgroups and urea appear for the SML molecules placed in water-urea medium depending on the SML concentration. In contrast, the number of the intermolecular hydrogen bonds between the sucrose headgroups and water molecules decreased by 1.3 on average at 2.5 and 5 wt% SML concentrations and about by ca. 0.5 for the higher SML concentrations studied. A high

impact on the number of intermolecular hydrogen bonds formed of the sucrose headgroups themselves was also observed in presence of urea. This number was found to decrease between 1.6 and 2.8 times, e.g. from 1.4 to 0.5 at 2.5 wt%, and from 2.0 to 1.3 at 40 wt%. This result explains why the final aggregates formed in the MD simulations performed in presence of urea experience a significantly decreased aggregation number and lower connectivity. Furthermore, it directly shows that hydrogen bonds formed between the sucrose headgroups are mainly responsible for the significantly increased viscosity of the solutions prepared without urea which have about 6-7 times higher relative viscosity (at 16 and 40 wt% concentration) compared to that of the solutions prepared with urea. However, note that the average number of hydrogen bonds between the sucrose headgroups does not diminish down to zero, which explains why even in presence of urea some supramicellar clusters are observed in the simulations, and also detected in the DLS measurements

Another direct indication that urea disrupts the strong interactions between the sucrose headgroups of separate primary micelles is the average distance between them. To quantify this effect, we measured these distances over the last 100 ns of the simulation for the system containing 2.5 wt% SML. A bimodal distribution of the distances over time is observed both in the absence and presence of urea with main maxima around 4 and 10 nm, see Fig. 7B. However, the peak intensities differ significantly in the two systems. In the absence of urea, the dominant peak occurs around 4 nm, whereas the main peak maximum shifts to approximately 10 nm in presence of urea. This result suggests that urea molecules forming hydrogen bonds with the sucrose headgroups situate between the primary micelles. In this way, the urea effectively maintains a greater distance between the individual micelles, preventing the formation of a strongly interconnected micellar network and consequently hindering the increase in viscosity observed in the concentrated solutions.

Aiming to get further insights into the structural arrangement of the formed micelles and the impact of urea on this arrangement, we performed a detailed structural analysis of isolating dimers of adjacent micelles formed during the simulations. Representative snapshots of the extracted aggregates from systems with 2.5 wt% SML, with and without urea, are shown as insets in Fig. 8A,B. The aggregate isolated from the simulation without urea consists of 206 molecules, organized into two spherical micelles containing 145 and 61 molecules. In contrast, the aggregate from the simulation with urea comprises 83 molecules, arranged into two micelles with 58 and 25 SML molecules. The aggregate formed in the absence of urea appears denser and more compact than that observed in the presence of urea. Furthermore, a clearly defined

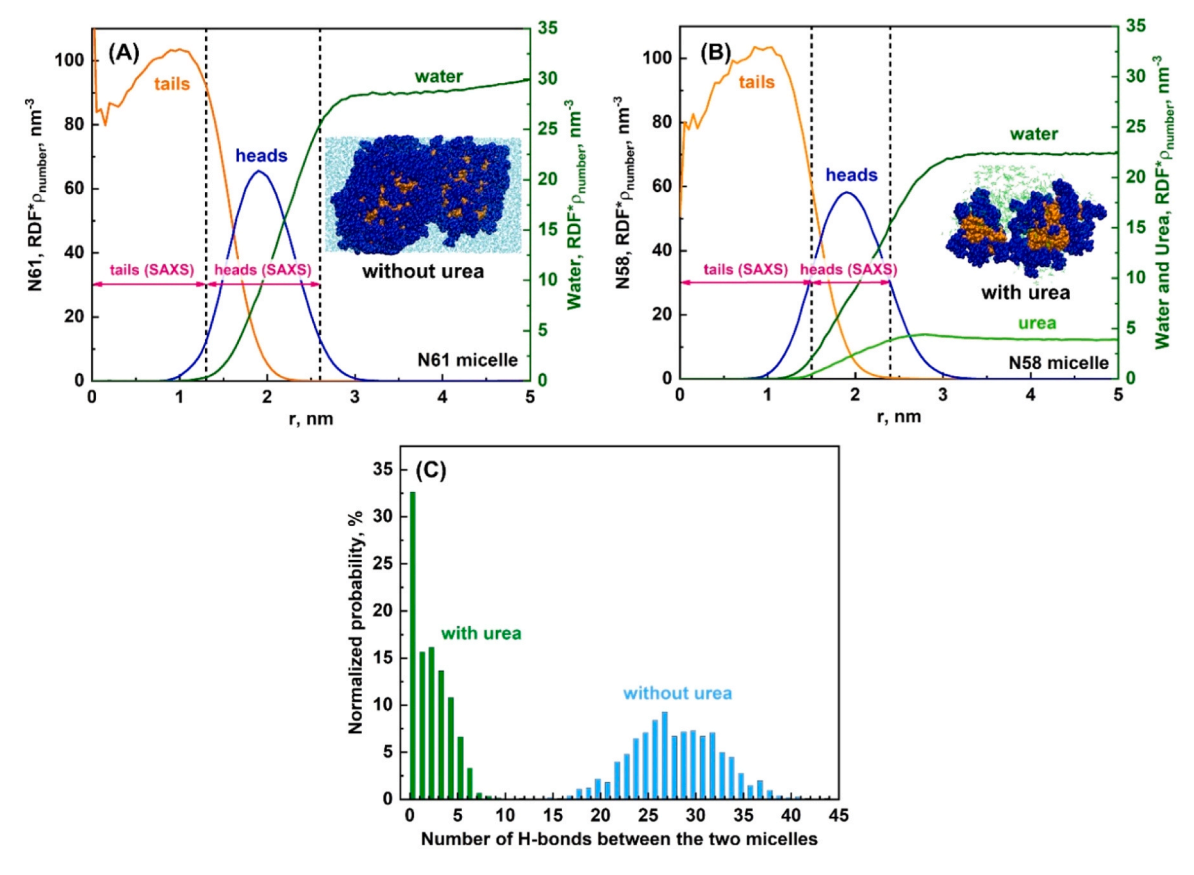


Fig. 8. Analysis of SML micelles obtained in 2.5 wt% SML simulations. (A,B) Radial distribution functions for micelles with: (A) 61 SML molecules from simulation without urea and (B) 58 SML molecules from simulation with urea. Insets show pictures from the isolated aggregates containing 206 SML and 83 SML molecules in total, respectively. The colors of the lines denote the RDFs for: alkyl tails – orange; sucrose heads – blue; water – dark green; urea – light green. Insets: pictures of the analyzed micelles. Blue balls denote sucrose heads, orange balls – alkyl tails, cyan sticks – water molecules, and green sticks – urea molecules. The vertical dashed lines in (A,B) denote the distances determined from the SAXS analysis at low surfactant concentrations. See also Supplementary Fig. S11. (C) Normalized probabilities for detection of a given number of intermolecular sucrose-sucrose hydrogen bonds formed between molecules from the two analyzed micelles in the aggregates. Green bars: simulation with urea; blue bars: simulation without urea.

layer of urea molecules is visible between the two micelles formed in the urea-containing system, preventing them from approaching each other more closely.

Molecular ordering within the isolated micelles was determined using the radial distribution functions (RDF) of the sucrose heads, alkyl tails, water, and urea molecules (when present), see Fig. 8A,B and Supplementary Figure S11. All distribution functions were calculated with respect to the geometrical center of the spherical micelles.

The structural arrangement was found to follow a layered organization in all investigated micelles, with alkyl tails forming the core, followed by the sucrose headgroups, and then the surrounding water molecules. This directly indicates that the sucrose heads are only partially hydrated, as it was also shown from the SASA analysis, Table 2 and from the SLD values for the shell determined from the SAXS analysis. In the presence of urea, the urea molecules are distributed throughout the aqueous phase, partially interacting with the sucrose headgroups. Note that the radial distribution functions are also in excellent agreement with the data determined from the SAXS analysis. In particular, from the SAXS spectra obtained in water, the equatorial core radius was determined to be  $R_{eq,core}\approx 13$  Å. This value coincides with the distance at which the RDF for the hydrocarbon tails decreases to 92 % of its maximal value, while the RDF for the sucrose headgroups increases to ca. 20 % of the maximal value, see vertical dashed line in Fig. 8A. Beyond this distance, the contribution from the sucrose headgroups becomes significant, and the SLD of the core can no longer be modeled as the one for dodecane. Furthermore, the shell thickness determined from the SAXS data in water is  $\approx 13\,\mbox{\normale}$  at surfactant concentrations  $\leq$  16 wt%. Adding this thickness to the equatorial core radius yields a total of 26 Å, a distance at which the RDF for the sucrose headgroups has decreased to ca. 20 % of its maximal value. At this point, the contribution from hydrating water molecules becomes dominant, and the scattering at larger distances is better modelled using the SLD of the pure solvent, see the vertical dashed line in Fig. 8A. Good agreement was also obtained between the RDFs of MD simulations and SAXS results for the system studied in presence of urea, see Fig. 8B.

The significantly altered interactions between the individual micelles were also evident from the number of hydrogen bonds formed between them, see Fig. 8C. In the absence of urea, about 30 intermolecular hydrogen bonds in total were observed between the two micelles. In contrast, in the presence of urea, only about two hydrogen bonds were detected between the two micelles formed. The significantly decreased number of hydrogen bonds formed between the micelles in presence of urea results from the ability of urea to form bonds with the sucrose headgroups, thus interrupting the intermolecular sucrose-sucrose bonding. This prevents to high extent the aggregation of the primary micelles in presence of urea, thus changing the properties of bulk L1695 solutions.

The results clearly demonstrate that hydrogen bonding between spherical micelles drives their aggregation, leading to an increase in viscosity while preserving Newtonian flow behavior across a wide range of shear rates. This indicates that, under the applied shear conditions, the characteristic time for micellar rearrangement exceeds that required for the breaking and reformation of intermicellar hydrogen bonds. In contrast to wormlike micellar systems – where increasing shear rate

typically disrupts the entangled network and markedly reduces apparent viscosity – the aggregated micelles studied here maintain stable viscosity even at high shear rates.

#### 4. Conclusions

In this study, we investigated systematically the self-assembly behavior of sucrose monolaurate (SML) in water across a concentration range of 1–40 wt%. All samples exhibited Newtonian rheological behavior. However, a pronounced increase in the viscosity of the aqueous solutions was observed at surfactant concentrations exceeding 20 wt%. This viscosity increase was accompanied by a corresponding rise in the intensity-weighted mean hydrodynamic diameter of the micelles present in the solutions.

Detailed investigations using X-ray scattering, DOSY NMR and atomistic molecular dynamics simulations revealed that SML forms nearly spherical micelles at low surfactant concentrations. These micelles largely preserve their individuality even at 40 wt%. However, at higher concentrations, hydrogen bonding between the sucrose headgroups promotes the formation of thread-like, interconnected structures. These aggregates resemble branched "pearl necklace" morphologies, previously reported for amphiphilic multiblock copolymers [51]. Notably, such structures have not been observed before in systems containing solely low-molecular-weight surfactants.

The role of hydrogen bonding for the formation of supra-micellar interconnected structures was further confirmed by studies conducted in the presence of 6 M urea, a known hydrogen bond disruptor. Sucrose monolaurate solutions prepared with urea exhibited significantly lower relative viscosities compared to those in pure water. Corresponding MD simulations showed reduced inter-micellar aggregation and decreased degree of structural organization. Clustering analysis further confirmed that urea reduced the size of micellar clusters, effectively suppressing the formation of large-scale assemblies.

This study reveals a previously unrecognized mechanism of spontaneous self-assembly in low molecular weight surfactants, mediated by extensive hydrogen bonding between surfactant headgroups. Although this behavior is demonstrated specifically for sucrose monolaurate, similar structures may be expected in other surfactant systems bearing multiple hydroxyl groups in their heads. Such molecules can form multiple intermicellar hydrogen bonds, resulting in an extensive intermicellar network, accompanied by a viscosity increase. Conversely, the presence of small hydrogen-bonding molecules such as urea, sugars, or monopropylene glycol, is expected to significantly affect this behavior. These molecules are likely to adsorb onto the micellar surface, thereby suppressing intermicellar hydrogen bonding and reducing the viscosity of the corresponding solutions. Future studies should explore the broader applicability of this self-assembly mechanism and investigate the influence of external factors such as pH, temperature, ionic strength, and co-solutes on the aggregation behavior.

# Funding

This study was funded by the European Union-NextGenerationEU, through the National Recovery and Resilience Plan of the Republic of Bulgaria, project No BG-RRP-2.004–0008.

## CRediT authorship contribution statement

N. Pagureva: Methodology, Investigation, Validation, Formal analysis, Visualization, Writing – original draft. F. Mustan: Methodology, Investigation, Validation, Formal analysis, Visualization, Writing – original draft. D. Cholakova: Methodology, Investigation, Validation, Formal analysis, Visualization, Writing – original draft, Writing – review & editing. N. Burdzhiev: Investigation, Validation. A. Ivanova: Methodology. S. Tcholakova: Conceptualization, Methodology, Supervision, Writing – review & editing, Funding acquisition.

#### **Declaration of Competing Interest**

The authors declare that they have no known competing financial interests or personal relationships that could have appeared to influence the work reported in this paper.

## Acknowledgements

The support of the Centre of Competence "Sustainable Utilization of Bio-resources and Waste of Medicinal and Aromatic Plants for Innova-Products" (BIORESOURCES BG16RFPR002-1.014-0001, funded by the Program "Research, Innovation and Digitization for Smart Transformation" 2021-2027, cofunded by the EU, is greatly acknowledged. The authors are grateful to Mitsubishi Chemical Corporation for the generous donation of L1695 Ryoto<sup>TM</sup>, allowing us to perform the experimental part of this study and to the Operational Program "Science and Education for Smart Growth" UNITe BG05M2OP001-1.001-0004-C01 contract No (2018-2023) and to the national Bulgarian supercomputer Discoverer for the allocated computational resources to perform the molecular dynamics simulations.

#### Appendix A. Supporting information

Supplementary data associated with this article can be found in the online version at doi:10.1016/j.colsurfa.2025.138915.

## Data availability

Data will be made available on request.

#### References

- [1] V.S. Nagtode, C. Cardoza, H.K.A. Yasin, S.N. Mali, S.M. Tambe, P. Roy, K. Singh, A. Goel, P.D. Amin, B.R. Thorat, J.N. Cruz, A.P. Pratap, Green surfactants (biosurfactants): a petroleum-free substitute for sustainability-comparison, applications, market, and future prospects, ACS Omega 8 (2023) 11674–11699, https://doi.org/10.1021/acsomega.3c00591.
- [2] A. Bhadani, A. Kafle, T. Ogura, M. Akamatsu, K. Sakai, H. Sakai, M. Abe, Current perspective of sustainable surfactants based on renewable building blocks, Curr. Opin. Colloid Interface Sci. 45 (2020) 124–135, https://doi.org/10.1016/j. cocis.2020.01.002.
- [3] R. Mori, Replacing all petroleum-based chemical products with natural biomassbased chemical products: a tutorial review, RSC Sustain. 1 (2023) 179–212, https://doi.org/10.1039/D2SU00014H.
- [4] J.-P. Zhu, M.-Y. Liang, Y.-R. Ma, L. White, M. Banwell, Y. Teng, P. Lan, Enzymatic synthesis of an homologous series of long- and very long-chain sucrose esters and evaluation of their emulsifying and biological properties, Food Hydrocoll. 124 (2022) 107149, https://doi.org/10.1016/j.foodhyd.2021.107149.
- [5] Y. Teng, S.G. Stewart, Y.-W. Hai, X. Lia, M. Banwell, P. Lan, Sucrose fatty acid esters: synthesis, emulsifying capacities, biological activities and structureproperty profiles, Crit. Rev. Food Sci. Nutr. 61 (2021) 3297–3317, https://doi.org/ 10.1080/10408398.2020.1798346.
- [6] L. Osipow, F.D. Snell, W.C. York, A. Finchler, Methods of preparation fatty acid esters of sucrose, Ind. Eng. Chem. 48 (1956) 1459–1462, https://doi.org/10.1021/ ie51400a026.
- [7] P.S. Deshpande, T.D. Deshpande, R.D. Kulkarni, P.P. Mahulikar, Synthesis of sucrose-coconut fatty acids esters: Reaction kinetics and rheological analysis, Ind. Eng. Chem. Res. 52 (2013) 15024–15033, https://doi.org/10.1021/ie401524g.
- [8] D. Cholakova, S. Tcholakova, Sucrose ester surfactants: Current understanding and emerging perspectives, Curr. Opin. Colloid Interface Sci. 73 (2024) 101832, https://doi.org/10.1016/j.cocis.2024.101832.
- [9] M. Verboni, D. Perinelli, C. Qiu, M. Tiboni, A. Aluigi, S. Lucarini, J. Lam, A. Duranti, Synthesis and properties of sucrose- and lactose-based aromatic ester surfactants as potential drugs permeability enhancers, Pharmaceuticals 16 (2023) 223, https://doi.org/10.3390/ph16020223.
- [10] T.L.T. da Silva, V. Baeten, S. Danthine, Modifying sucrose esters oleogels properties using different structuration routes, Food Chem. 405 (2023) 134927, https://doi. org/10.1016/j.foodchem.2022.134927.
- [11] B.-B.C. Youan, A. Hussain, N.T. Nguyen, Evaluation of sucrose esters as alternative surfactants in microencapsulation of proteins by the solvent evaporation method, AAPS Pharm. Sci. 5 (2003) 22, https://doi.org/10.1208/ps050222.
- [12] Y. Ning, L. Hou, M. Ma, M. Li, Z. Zhao, D. Zhang, Z. Wang, Y. Jia, Synergistic antibacterial mechanism of sucrose laurate combined with nisin against Staphylococcus aureus and its application in milk beverage, LWT 158 (2022) 113145, https://doi.org/10.1016/j.lwt.2022.113145.

- [13] M.N. Todosijević, G. Brezesinski, S.D. Savić, R.H.H. Neubert, Sucrose esters as biocompatible surfactants for penetration enhancement: an insight into the mechanism of penetration enhancement studied using stratum corneum model lipids and Langmuir monolayers, Eur. J. Pharm. Sci. 99 (2017) 161–172, https://doi.org/10.1016/j.eips.2016.12.002.
- [14] V. Molinier, P. Kouwer, J. Fitremann, A. Bouchu, G. Mackenzie, Y. Queneau, J. Goodby, Self-organizing properties of monosubstituted sucrose fatty acid esters: the effects of chain length and unsaturation, Chem. A Eur. J. 12 (2006) 3547–3557, https://doi.org/10.1002/chem.200500773.
- [15] B.A.P. Nelen, L. Bax, J.M. Cooper, Chapter 7: Sucrose esters, in: V. Norn (Ed.), Emulsifiers in Food Technology, Wiley Online Library, 2014, pp. 147–180, https://doi.org/10.1002/9781118921265.ch7
- [16] L.N. Scott, W.F. Bergfeld, D.V. Belsito, R.A. Hill, C.D. Klaassen, D.C. Liebler, J. G. Marks Jr, R.C. Shank, T.J. Slaga, P.W. Snyder, L.J. Gill, B. Heldreth, Safety assessment of saccharide esters as used in cosmetics, Int. J. Toxicol. 40 (2021) 528–1165, https://doi.org/10.1177/10915818211016378.
- [17] H. Maag, Fatty acid derivatives: Important surfactants for household, cosmetic and industrial purposes, J. Am. Oil Chem. Soc. 61 (1984) 259–267, https://doi.org/ 10.1007/BF02678778
- [18] A. Szűts, P. Szabó-Révész, Sucrose esters as natural surfactants in drug delivery systems—A mini-review, Int. J. Pharm. 433 (2012) 1–9, https://doi.org/10.1016/j. ijpharm.2012.04.076.
- [19] B.A.P. Nelen, J.M. Cooper, Sucrose esters, in: R.J. Whitehurst (Ed.), Emulsifiers in food technology, Blackwell Publishing Ltd, Northampton, UK, 2004, pp. 131–161.
- [20] X. Hu, B. Binks, Z. Cui, Edible oil-in-water emulsions stabilized by hydrophile-lipophile balanced sucrose ester, J. Am. Oil Chem. Soc. 100 (2023) 711–721, https://doi.org/10.1002/aocs.12698.
- [21] T. Herrington, S. Sahi, Phase behavior of some sucrose surfactants with water and n-decane, J. Am. Oil Chem. Soc. 65 (1988) 1677–1681, https://doi.org/10.1007/ BF02912575.
- [22] Y. Ishigami, H. Machida, Vesicles from sucrose fatty acid esters, J. Am. Oil Chem. Soc. 66 (1989) 599–603, https://doi.org/10.1007/BF02885457.
- [23] C. Calahorro, J. Muñoz, M. Berjano, A. Guerrero, C. Gallegos, Flow behavior of sucrose stearate/water systems, J. Am. Oil Chem. Soc. 69 (1992) 660–666, https:// doi.org/10.1007/BF02635806.
- [24] M. Yamamoto, H. Ando, S. Arima, K. Aramaki, Rheological properties of wormlike micelles solutions being available in wide temperature range in sucrose palmitate systems, J. Oleo Sci. 58 (2009) 303–311, https://doi.org/10.5650/jos.58.303.
- [25] A. Szűts, M. Budai-Szűcs, I. Erős, N. Otomo, P. Szabó-Révész, Study of gel-forming properties of sucrose esters for thermosensitive drug delivery systems, Int. J. Pharm. 383 (2010) 132–137, https://doi.org/10.1016/j.ijpharm.2009.09.013.
- [26] K. Aramaki, S. Hoshida, S. Arima, Formation of wormlike micelles with natural-sourced ingredients (sucrose fatty acid ester and fatty acid) and a viscosity-boosting effect induced by fatty acid soap, Colloids Surf. A Physicochem. Eng. Asp. 396 (2012) 278–282, https://doi.org/10.1016/j.colsurfa.2012.01.009.
- [27] S. Takahashi, I. Kaneda, A transient network structure in sucrose stearate/water systems, Nihon Reoroji Gakkaishi J. Soc. Rheol. Jpn. 42 (2014) 103–109, https:// doi.org/10.1678/rheology.42.103.
- [28] N. Pagureva, D. Cholakova, Z. Mitrinova, M. Hristova, N. Burdzhiev, S. Tcholakova, Temperature response of sucrose palmitate solutions: Role of ratio between monoesters and diesters, J. Colloid Interface Sci. 674 (2024) 209–224, https://doi.org/10.1016/j.jcis.2024.06.061.
- [29] N. Pagureva, M. Hristova, S. Tcholakova, D. Cholakova, Salt-induced gelation of nonionic sucrose ester dispersions, J. Colloid Interface Sci. 693 (2025) 137610, https://doi.org/10.1016/j.jcis.2025.137610.
- [30] M. Berjano, A. Guerrero, J. Muñoz, C. Gallegos, Temperature dependence of viscosity for sucrose laurate/water micellar systems, Colloid Polym. Sci. 271 (1993) 600–606. https://doi.org/10.1007/BF00657991.
- [31] L. Delforce, S. Tcholakova, Alkyl sucrose esters vs. Brijs: How, chain Length Temp. Impact Surf. Foam Prop. J. Mol. Liq. 416 (2024) 126491, https://doi.org/10.1016/j.mollig.2024.126491.
- [32] A.D. Becke, Density-functional exchange-energy approximation with correct asymptotic behavior, Phys. Rev. A At. Mol. Opt. Phys. 38 (1988) 3098–3100, https://doi.org/10.1103/PhysRevA.38.3098.
- [33] A.D. Becke, Density-functional thermochemistry. III, role Exact. Exch. J. Chem. Phys. 98 (1993) 5648–5652, https://doi.org/10.1063/1.464913.
- [34] R. Ditchfield, W.J. Hehre, J.A. Pople, Self-consistent molecular-orbital methods. IX, Ext. GaussianType basis Mol. Orbit Stud. Org. Mol. J. Chem. Phys. 54 (1971) 724–728, https://doi.org/10.1063/1.1674902.
- [35] P. Raman, O. Guvench, A.D. MacKerell Jr., CHARMM additive all-atom force field for glycosidic linkages in carbohydrates involving furanoses, J. Phys. Chem. B 114 (2010) 12981–12994, https://doi.org/10.1021/jp105758h.
- [36] J.B. Klauda, R.M. Venable, J.A. Freites, J.W. O'Connor, D.J. Tobias, et al., Update of the CHARMM all-atom additive force field for lipids: validation on six lipid types, J. Phys. Chem. B 114 (2010) 7830–7843, https://doi.org/10.1021/ in101759a
- [37] O. Guvench, E.R. Hatcher, R.M. Venable, R.W. Pastor, R.W, A.D. MacKerell Jr., Additive empirical CHARMM force field for glycosyl linked hexopyranoses. J. Chem. Theory, Comp 5 (2009) 2353–2370, https://doi.org/10.1021/ct900242e.

- [38] W.L. Jorgensen, J. Chandrasekhar, J.D. Madura, R.W. Impey, M.L. Klein, Comparison of simple potential functions for simulating liquid water, J. Chem. Phys. 79 (1983) 926–935, https://doi.org/10.1063/1.445869.
- [39] C. Zhu, R.H. Byrd, P. Lu, J. Nocedal, Algorithm 778: L-BFGS-B, Fortran routines for large scale bound constrained optimization, ACM Trans. Math. Softw. (TOMS) 23 (1997) 550–560, https://doi.org/10.1145/279232.279236.
- [40] G. Bussi, D. Donadio, M. Parrinello, M, Canonical sampling through velocity rescaling, J. Chem. Phys. 126 (2007) 014101, https://doi.org/10.1063/ 1.2408420.
- [41] H.J.C. Berendsen, J.P.M. Postma, W.F. van Gunsteren, A. DiNola, J.R. Haak, Molecular-dynamics, coupling Extern. Bath. J. Chem. Phys. 81 (1984) 3684–3690, https://doi.org/10.1063/1.448118.
- [42] R.W. Hockney, S.P. Goel, J. Eastwood, Quiet high-resolution computer models of a plasma, J. Comp. Phys. 14 (1974) 148–158, https://doi.org/10.1016/0021-9991 (74)90010-2
- [43] J.-P. Ryckaert, G. Ciccotti, H.J.C. Berendsen, Numerical integration of the Cartesian equations of motion of a system with constraints: molecular dynamics of n, alkanes J. Comput. Phys. 23 (1977) 327–341, https://doi.org/10.1016/0021-9991(77)90098-5.
- [44] S. Miyamoto, P.A. Kollman, Settle: An analytical version of the SHAKE and RATTLE algorithm for rigid water models, J. Comput. Chem. 13 (1992) 952–962, https://doi.org/10.1002/jcc.540130805.
- [45] T. Darden, D. York, L. Pedersen, Particle mesh Ewald: An N-log(N) method for Ewald, sums Large Syst. J. Chem. Phys. 98 (1993) 10089–10092, https://doi.org/ 10.1063/1.464397
- [46] U. Essmann, L. Perera, M.L. Berkowitz, T. Darden, H. Lee, L.G. Pedersen, A smooth particle mesh Ewald method, J. Chem. Phys. 103 (1995) 8577–8593, https://doi. org/10.1063/1.470117.
- [47] Abraham Lindahl, Hess, van der Spoel, GROMACS 2021.3 Manual (2021.3), Zenodo (2021), https://doi.org/10.5281/zenodo.5053220.
- [48] W. Humphrey, A. Dalke, K. Schulten, VMD: Visual Molecular Dynamics, J. Mol. Graph. 14 (1996) 33–38, https://doi.org/10.1016/0263-7855(96)00018-5.
- [49] C.M. Maguire, M. Rösslein, P. Wick, A. Prina-Mello, Characterisation of particles in solution – a perspective on light scattering and comparative technologies, Sci. Techn. Adv. Mat. 19 (2018) 732–745, https://doi.org/10.1080/ 14686996, 2018.1517587.
- [50] S. Fall, B. Pattier, L. Benyayia, A. Gibaud, Binary phase diagram of water/Brij 58 studied by SAXS, Acta Phys. Pol. A 121 (2012) 388–396, https://doi.org/ 10.12693/APhysPolA.121.388.
- [51] V. Hugouvieux, M.A.V. Axelos, M. Kolb, Micelle formation, gelation and phase separation of amphiphilic multiblock copolymers, Soft Matter 7 (2011) 2580–2591, https://doi.org/10.1039/c0sm01018a.
- [52] D.W. Bolen, G.D. Rose, Structure and energetics of the hydrogen-bonded backbone in protein folding, Ann. Rev. Biochem 77 (2008) 339–362, https://doi.org/ 10.1146/annurey.biochem.77.061306.131357.
- [53] R. Zangi, R. Zhou, B.J. Berne, Urea's action on hydrophobic interactions, J. Am. Chem. Soc. 131 (2009) 1535–1541, https://doi.org/10.1021/ja807887g.
- [54] W.K. Lim, J. Rösgen, S. W.r Englander, Urea, but not guanidinium, destabilizes proteins by forming hydrogen bonds to the peptide group, PNAS 106 (2009) 2595–2600, https://doi.org/10.1073/pnas.0812588106.
- [55] L. Delforce, S. Tcholakova, Role of temperature and urea for surface and foam properties of nonionic surfactants with dodecyl alkyl chain, Colloids Surf. A 691 (2024) 133844, https://doi.org/10.1016/j.colsurfa.2024.133844.
- [56] P.K. Das Gupta, S.P. Moulik, Effects of urea and a nonionic surfactant on the micellization and counterion binding properties of cetyltrimethyl ammonium bromide and sodium dodecyl sulfate, Colloid Polym. Sci. 267 (1989) 246–254, https://doi.org/10.1007/BF01410582.
- [57] M.J. Schick, 1964, Effect of electrolyte and urea on micelle formation, J. Phys. Chem. 68 (1964) 3585-3592. https://doi.org/10.1021/j100794a025.
- [58] G. Briganti, S. Puvvada, D. Blankschtein, Effect of urea on micellar properties of aqueous solutions of nonionic surfactants, J. Phys. Chem. 95 (1991) 8989–8995, https://doi.org/10.1021/j100175a103.
- [59] C.L. Bianco, C.S. Schneider, M. Santonicola, A.M. Lenhoff, E.W. Kaler, Effects of urea on the microstructure and phase behavior of aqueous solutions of poly (oxyethylene) surfactants, Ind. Eng. Chem. Res. 50 (2011) 85–96, https://doi.org/ 10.1021/ie101011v.
- [60] S. Zendenhroud, J.O. Daldrop, Y. von Hansen, H. Kiefer, R.R. Netz, Molecular Stokes-Einstein and Stokes-Einstein-Debye relations for water including viscositydependent slip and hydrodynamic radius, Phys. Rev. E 110 (2024) 064610, https://doi.org/10.1103/PhysRevE.110.064610.
- [61] R.J. BaxterPercus-Yevick equation for hard spheres with surface adhesion, J. Chem. Phys. 49 (1968) 2770-2774. https://doi.org/10.1063/1.16704821968, 2770277410.1063/1.1670482.
- [62] P.T. Cummings, J.W. Perram, E.R. Smith, Percus-Yevick theory of correlation functions and nucleation effects in the sticky hard-sphere model, Mol. Phys. A 31 (1976) 535–548, https://doi.org/10.1080/00268977600100411.
- [63] S.V.G. Menon, C. Manohar, S. Srinivasa Rao, A new interpretation of the sticky hard sphere model, J. Chem. Phys. 95 (1991) 9186–9190, https://doi.org/ 10.1063/1.461199.